Photochemical & Photobiological Sciences (2023) 22:1875–1888
https://doi.org/10.1007/s43630-023-00418-0

ORIGINAL PAPERS

Toward combined photobiological–photochemical formation of kerosene-type biofuels: which small 1,3-diene photodimerizes most efficiently?

Sindhujaa Vajravel[1] · Leandro Cid Gomes[1] · Anup Rana[1] · Henrik Ottosson[1]

Received: 8 February 2023 / Accepted: 3 April 2023 / Published online: 26 April 2023

Abstract

A transition from fossil- to bio-based hydrocarbon fuels is required to reduce greenhouse gas emissions; yet, traditional biomass cultivation for biofuel production competes with food production and impacts negatively on biodiversity. Recently, we reported a proof-of-principle study of a two-step photobiological–photochemical approach to kerosene biofuels in which a volatile hydrocarbon (isoprene) is produced by photosynthetic cyanobacteria, followed by its photochemical dimerization into C_{10} hydrocarbons. Both steps can utilize solar irradiation. Here, we report the triplet state (T_1)-sensitized photodimerization of a broader set of small 1,3-dienes to identify which structural features lead to rapid photodimerization. Neat 1,3-cyclohexadiene gave the highest yield (93%) after 24 h of irradiation at 365 nm, followed by isoprene (66%). The long triplet lifetime of 1,3-cyclohexadiene, which is two orders of magnitude longer than those of acyclic dienes, is key to its high photoreactivity and stem from its planar T_1 state structure. In contrast, while isoprene is conformationally flexible, it has both photochemical and photobiological advantages, as it is the most reactive among the volatile 1,3-dienes and it can be produced by cyanobacteria. Finally, we explored the influence of solvent viscosity, diene concentration, and triplet sensitizer loading on the photodimerization, with a focus on conditions that are amenable when the dienes are produced photobiologically. Our findings should be useful for the further development of the two-step photobiological–photochemical approach to kerosene biofuels.

Graphical abstract

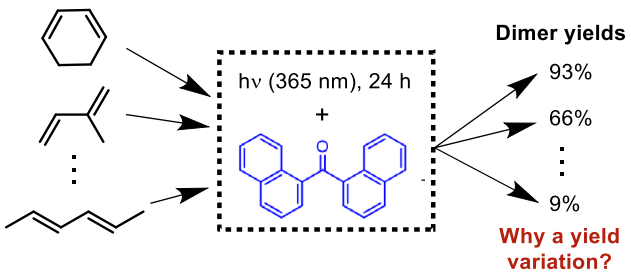

1 Introduction

Small alkenes and conjugated dienes are essential building blocks in the petrochemical industry. They can be oligomerized into larger hydrocarbon chains to produce energy-dense fuels in the range C_8–C_{16} suitable for jet fuels [1]. Today, small conjugated dienes are mainly produced as by-products in the production of ethylene through steam cracking of fossil-based naphtha [2, 3]. Thus, great attention has recently

Sindhujaa Vajravel and Leandro Cid Gomes contributed equally to the investigation.

✉ Henrik Ottosson
henrik.ottosson@kemi.uu.se

[1] Department of Chemistry-Ångström Laboratory, Uppsala University, Box 523, 751 20 Uppsala, Sweden

been directed to more sustainable routes to small bio-based conjugated dienes through direct production from living organisms (e.g., microbes, algae, and plants) as well as from biomass-derived sugars and plant oils [4].

The direct biotechnological production of C_8–C_{16} hydrocarbons by microbes is possible [5–8]; however, this process is limited due to the toxicity of these hydrocarbons as they accumulate in the cells and interfere with the cell membrane integrity [9]. Besides this, the extraction and purification processes of large molecules require energy-intensive procedures leading to increased production costs. As an alternative method to overcome these complicating issues, we recently proposed a two-step photobiological–photochemical approach where photosynthetic cyanobacteria produce volatile isoprene directly from CO_2, water, and (solar) light, followed by its photochemical dimerization into C_{10} monoterpenoids [10]. The second step is a triplet-sensitized photodimerization that also can be run by solar light. Indeed, the triplet state photosensitized dimerization of conjugated dienes is an established approach within organic photochemistry to produce [2 + 2], [4 + 2] and [4 + 4] cycloadducts [11–15], and after hydrogenation, the cycloadducts are attractive as kerosene-type fuels with high energy density [16]. A life cycle assessment of our photobiological–photochemical approach to biojet fuels via isoprene indicated that the climate change impact was about 20% that of fossil-based jet fuels [10]. Now, can this method be applied also for, e.g., 1,3-butadiene?

The general approach of the fourth generation of biofuels is to use genetically modified photosynthetic microorganisms to produce organic compounds directly from CO_2, water, and sunlight (Fig. 1), which avoids biomass cultivation, harvesting, and processing [17, 18]. Recent advances in the metabolic engineering of cyanobacteria have been reported to produce short-chain olefins [19, 20], including isoprene [21]. One may also go via even shorter hydrocarbons, e.g., ethylene produced photosynthetically [19, 22], to form conjugated dienes such as 2,4-hexadiene [23]. Furthermore, metabolically engineered non-photosynthetic microbes can produce other conjugated dienes (e.g., 1,3-butadiene) and trienes [24, 25], and incorporation of the corresponding genes into photosynthetic microorganisms might be a viable route.

While the direct photosynthetic production of 1,3-dienes by microbes is still in its early stages with too low production rate of dienes for large-scale applications [21], these compounds can also be produced through biomass processing (Fig. 1). Plant oil derivatives and microalgal lipids have been used for a range of chemical transformations, including oligomerizations and olefin metathesis [26]. The latter can produce 1,4-cyclohexadiene as a common by-product [27, 28], and this compound can be further converted to 1,3-cyclohexadiene via photoisomerization [29–31]. Besides the biological production of 1,3-cyclohexadiene, other industrially important dienes can be produced via a number of renewable approaches, including (*i*) catalytic conversion of bio-derived ethanol, C_4 alcohols, and diols to produce 1,3-butadiene, [3, 32] (ii) bio-based production of 2,3-dimethyl-1,3-butadiene by acid-catalyzed dehydration of pinacol in ionic liquids [33], and (iii) 1,3-pentadiene production from lignocellulose biomass [34, 35]. Although several studies focused on the production of dienes from the fermentation of biomass sugars, none of the pathways have been commercialized for industrial production.

Taken together, several (photo)biological approaches are being developed for the production of conjugated dienes. Likewise, several methods for the conversion of small hydrocarbons into fuels exist, spanning from traditional and commercially established C–C bond-forming reactions, e.g., Fisher–Tropsch synthesis and acid-catalyzed oligomerization [36, 37], to the more recently developed thermal and/or metal-catalyzed reactions [38, 39]. From a sustainability

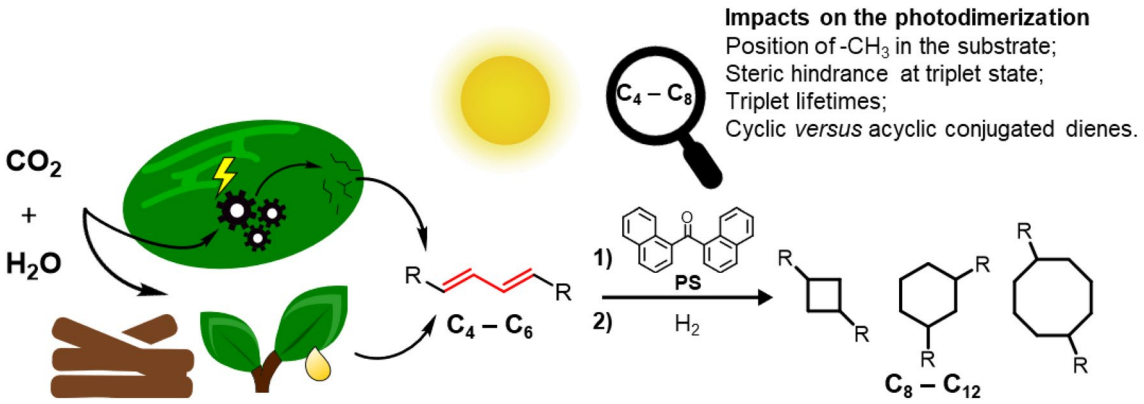

Fig. 1 Our principle of the combined photobiological and photochemical production of C_8–C_{12} hydrocarbons from CO_2, together with the aspects investigated in this work. Sources represented: photosynthetic microorganisms, lignocellulose (for fermentation), and plant oils. See the main text for further details. PS = photosensitizer, 1,1-dinaphthylmethanone

perspective, the routes to oligomerize small hydrocarbons need to be further developed to reduce the environmental impact. Here, photochemical oligomerization reactions triggered by visible or near-ultraviolet light have significant importance for the development of such routes, as these reactions can utilize sunlight as the main energy source. In this context, we recently revealed that mono- and sesquiterpenes with conjugated diene units can be photodimerized with solar light to products that can serve as biodiesel and lubricant oils [40]. Thus, even though small and volatile 1,3-dienes can be especially suitable for biotechnological production using photosynthetic microorganisms. There is also a diversity of renewable sources of small conjugated dienes. Combined with their sunlight-driven photodimerization, this can be a route to reduce the environmental impact of jet fuel production.

To guide future photobiological work, we now seek to find out which conjugated dienes are easiest to transform photochemically into their dimers and asked the following questions: How do the substituents and the structures of the 1,3-dienes affect the photochemical dimerization? What are the main factors affecting the triplet-sensitized photodimerization? Can another small conjugated diene than isoprene provide for a more efficient photodimerization? We utilized 1,1-dinaphthylmethanone as photosensitizer (**PS**, Fig. 1), as it has been identified as a suitable photosensitizer under solar irradiation [10, 40, 41]. The effects of solvent viscosity, dilution, and photosensitizer loading on the dimerization yields were also mapped out, and these factors were optimized considering conditions that are relevant for photobiological diene production. Our work can provide insights that will benefit future efforts on the combined photobiological–photochemical production of kerosene-type biofuels.

2 Experimental

2.1 Materials

Isoprene (mass purity > 99%), 2,3-dimethyl-1,3-butadiene (98%), *E*-1,3-pentadiene (90%), 2,4-hexadiene (90%), 1,3-butadiene (15 wt. % in hexane), 3-methyl-1,3-pentadiene (98%), 1,3-cyclohexadiene (97%), 1,3-cycloheptadiene (95%), and *Z*,*Z*-1,3-cyclooctadiene (97%) were obtained from Sigma-Aldrich. All chemicals were directly used as received unless mentioned otherwise. Before the photochemical reaction, *tert*-butyl catechol was removed from the following dienes: isoprene, 2,3-dimethyl-1,3-butadiene, and 1,3-cyclohexadiene. 1,1-Dinaphthylmethanone was synthesized according to previous reported literature. [10] Noteworthy, the hexane solution of 1,3-butadiene did not contain any stabilizer.

2.2 Photosensitized dimerization of conjugated dienes

An inhibitor (*tert*-butyl catechol)-free liquid diene was mixed with 1,1-dinaphthylmethanone (photosensitizer used in the range of 0.1–0.5 mol%). Two different volumes of reaction solutions were used in this study: 5 mL in all the experiments with neat dienes (> 90 wt%); and 20 mL for reactions of diluted dienes (< 60 wt%). A solution of diene and photosensitizer was then degassed by using freeze–pump–thaw cycles (3 ×) and left in an argon atmosphere. By using a syringe, the homogenous solution was then transferred to the coiled tube reactor (Teflon tube O.D. × I.D.: 3.18 mm × 2.1 mm, loop size ~ 20 mL) [10] sealed with septa. The reactor had been previously purged with argon gas for 3 min. The coiled tube reactor was then connected to the chiller at a constant temperature (7 °C) to maintain the reaction at a low temperature to avoid the build-up of pressure or loss of starting material. Either an RPR-100 or -200 Rayonet Photochemical Chamber reactor was used for the photoreaction. The photochemical reaction was initiated under irradiation at 365 nm (Xenon lamp, 16 × 24 WUV lamp purchased from Southern New England Ultraviolet Company) and run for 24 h (if not mentioned otherwise). The light intensity in the reactor was approximately 8 mW/cm^2 (if not mentioned otherwise) as measured by a portable radiometer (spectral radiometer RM12 purchased from Opsytec). After the reaction time, the solution was passed through a silica gel column using pentane as the eluent. The diene dimers were separated by distillation under reduced pressure.

2.3 Characterization of reaction products

An Agilent 7890A GC and 5975 MSD system was used for monitoring the photoreactions, using split injection (1 µL injection volume; split ratio: 100:1; 250 °C inlet temperature; flow rate: 120 mL/min) and capillary column (19091S-433: 325 °C: 30 m × 250 µm × 0.25 µm (front SS inlet: He; out: vacuum)). The initial temperature of the column oven was 70 °C (0.5 min equilibration time) and the final temperature of the sample run was 320 °C. The rate of temperature was set to 20 °C/min resulting in a 12.5 min total run time. Helium gas was used as a carrier gas at a flow rate of 1.2 mL/min. The source and Quad temperatures of the mass spectrometer are, respectively, 230 and 150 °C. The total yield of dimers was determined gravimetrically. The ^{1}H NMR spectra were recorded on a JEOL (400YH magnet) Resonance 400 MHz spectrometer. Chemical shifts δ are reported in ppm and coupling constants J in Hz. ^{1}H NMR

chemical shifts are referenced to the residual solvent signal ($CDCl_3$, ^1H 7.26 ppm).

2.4 Computational methods

Geometry optimizations were performed with Gaussian16 at the (U)B3LYP-D3/6-311 + G(d,p) level [42–45]. Triplet states were calculated with the unrestricted Kohn–Sham DFT formalism. Stationary points were characterized as minima or transition states through frequency calculations. The Gibbs free energies used in the mechanistic investigation were calculated at 298 K.

3 Results and discussion

Our analysis starts with the combined experimental and computational exploration of structural effects on the photodimerization of acyclic 1,3-dienes, before analyzing cyclic 1,3-dienes. Subsequently, we probe photodimerizations of dilute solutions of isoprene and the effects of triplet sensitizer loadings and solvent viscosity.

3.1 Structural effects of 1,3-diene photodimerizations

A series of different 1,3-dienes were selected (**1**–**9**, Fig. 2) to investigate the effects of molecular structure on the photosensitized dimerization. We first focused on **1**–**7**. This set of compounds allows us to explore the effects of (i) increasing the number of methyl substituents, (ii) the position of the methyl substituents on the conjugated diene, i.e., substitution at the central C_2/C_3 atoms versus the terminal C_1/C_4 atoms, and (iii) acyclic versus cyclic structures. Not all dienes **1**–**7** are volatile, yet with these we can assess the structural effects on triplet-sensitized photodimerizations of 1,3-dienes. Noteworthy, there is a fourth dimethyl-1,3-butadiene isomer, 2-methyl-1,3-pentadiene; however, it is not readily available and has a boiling point of 78 °C. It was therefore excluded. In a later section, we discuss the larger cycloalka-1,3-dienes **8** and **9** in their T_1 states to probe the effect of ring size on the twisting of the diene segments and its impact on the diene dimerization yields (vide infra). We did not consider the small 1,3-cyclopentadiene as it dimerizes thermally within hours via the Diels–Alder reaction.

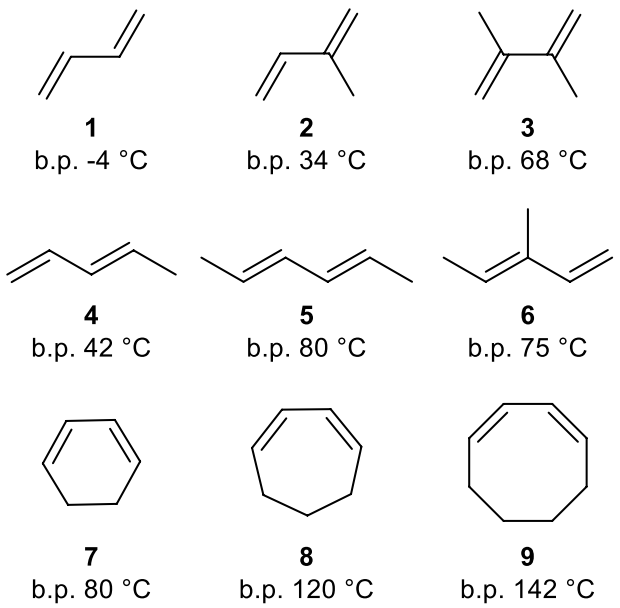

Fig. 2 The 1,3-dienes investigated in this study and their boiling points (b.p.): 1,3-butadiene **1,** isoprene **2**, 2,3-dimethyl-1,3-butadiene **3**, *E*-1,3-pentadiene **4**, 2,4-hexadiene **5**, 3-methyl-1,3-pentadiene **6**, 1,3-cyclohexadiene **7**, 1,3-cycloheptadiene **8**, *Z,Z*-1,3-cyclooctadiene **9**

The triplet energies, $E(T_1)$, of the conjugated dienes **1**–**7** and the photosensitizer 1,1-dinaphthylmethanone at (U)B3LYP-D3/6-311 + G(d,p) level are listed in Table 1. Since we utilized a mixture of *Z*- and *E*-isomers in the experiments with **5** and **6**, we computed $E(T_1)$ of all the isomers present. The $E(T_1)$ of 1,1-dinaphthylmethanone (52.2 kcal mol^{-1}) is slightly higher than those of the dienes studied herein, making it a suitable sensitizer in our studies. The triplet lifetime of 1,1-dinaphthylmethanone is 300 ns, [41] which is long enough for molecular collisions and energy transfer to take place. Furthermore, the T_1 state of 1,1-dinaphthylmethanone has a $\pi\pi^*$ character, which prevents the competing H-atom abstraction pathway [46].

All dimerization reactions were run in a Teflon tube coiled around a water-cooled condenser (Fig. 3), using neat dienes, except for 1,3-butadiene (**1**) which was run dilute in hexane, i.e., the form in which it is commercially available. Photoirradiations of dienes **2**–**7** with a 0.1 mol% photosensitizer loading ($\lambda = 365$ nm, $t = 24$ h) gave the dimer yields reported in Table 1. Considering that the photosensitizer 1,1-dinaphthylmethanone is kept throughout this study, and for an applications point of view, we base our comparisons on the yields of the dimer products and not on the quantum yields.

The formation of dimers in all irradiated samples could be confirmed through GC–MS analyses (Figs. S1–S3, ESI). Trace amounts of trimers were found for **7** and **2** (Fig. S4, ESI), and the photosensitizer was preserved in the irradiated samples, without formation of H-atom abstraction products (*i.e.* di(naphthalen-1-yl)methanol, Fig. S5, ESI). Interestingly, a varying degree of selectivity in the photodimerizations is observed in the chromatograms since some dienes produced a larger number of different dimer isomers than others (Figs. S1–S3, ESI). In the case of **5**, the large number of dimer isomers in the products can be traced back to the different isomers in the starting material. Considering

Table 1 Triplet state energies of small 1,3-dienes and the photodimerization yields (0.1 mol% 1,1-dinaphthylmethanone), using neat dienes unless otherwise stated

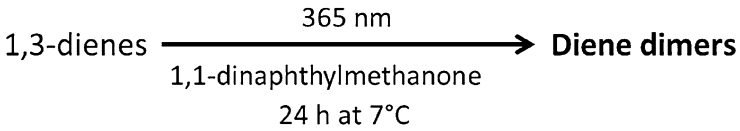

Compound number	Diene	Computed $E(T_1)$ (kcal mol^{-1})[a]	Dimer yield (wt%)
1	1,3-Butadiene	50.4	(6.5)[e]
2	Isoprene	49.8	66 (18)[e]
3	2,3-Dimethyl-1,3-butadiene	50.1	29
4	*E*-1,3-Pentadiene	49.7	20
5	2,4-Hexadiene	46.4[b]/47.3[c]/49.4[d]	9 (1.0)[e]
6	3-Methyl-1,3-pentadiene	46.7[f]/47.2[g]	9
7	1,3-Cyclohexadiene	46.4	93
8	1,3-Cycloheptadiene	48.9	45
9	*Z,Z*-1,3-Cyclooctadiene	45.1	7

[a]Calculated at (U)B3LYP-D3/6-311 + G(d,p) level with thermal free energy corrections at 298 K. [b]*Z,Z*-isomer. [c]*E,Z*-isomer. [d]*E,E*-isomer. [e]Yield in parenthesis when diluted diene samples (15 wt% in hexane) are used. [f]*Z*-isomer. [g]*E*-isomer

Fig. 3 The coiled Teflon tube around the water-cooled condenser is used for the photodimerization reaction of dienes. The reaction was run at ~ 7 °C. The starting experimental solutions containing diene and 1,1-dinaphthylmethanone mixture were transferred into the Teflon tube and both ends were sealed with rubber septa

that we are interested in the total yield of dimers, we do not assess the specific structures of each of the dimers produced. Earlier studies have explored the structure of dimers in detail for some of the 1,3-dienes, and found that photosensitized dimerization of isoprene, 1,3-cyclohexadiene, and 2,3-dimethyl-1,3-butadiene were observed as, respectively, seven, three, and seven different dimers [11, 13]. The compositions of these product mixtures (dimer isomers) were strongly dependent on the photosensitizers employed and on the distribution between the available diene conformers in the S_0 state [11, 13]. Interestingly, the various 1,3-dienes exhibit a wide range in the yields of their dimers, spanning from 93% down to values below 9%. Among the acyclic dienes that can be used neat (**2**–**6**), **2** displayed the highest yield, followed by **3** and **4**, while the lowest was obtained for **5** and **6** (both ~ 9%). At this point, it can be noted that **5** exhibits also a low quantum yield of sensitized *Z*/*E*-photoisomerization. [47]

The 1,3-butadiene photodimerization could only be run in hexane solution (15 wt.% as commercially available), and the observed yield was merely 6.5%. Now, when **2** and **5** (the most and the least reactive acyclic diene, respectively) were run in hexane under the same conditions as those of **1**, the yield of dimers of **2** was still higher (18%) than that of **1**, but that of **5** decreased from 9 to 1% (Table 1, footnote e). These results show that **5** is much less reactive than **1**, and together with **6**, the least reactive of the acyclic 1,3-dienes. As **2** still gives the highest yield among our selected small acyclic 1,3-dienes, it becomes apparent that **2** has advantages over **1** from a photochemical point of view, besides that it already can be produced photobiologically. A potential benefit of **1** could be that it should evaporate more easily from the cells than **2**.

Next, we used DFT computations to identify the reasons for the different reactivities among the investigated 1,3-dienes. The reaction mechanism of the photosensitized dimerization of conjugated dienes can be seen as a sequence of three major steps, as depicted in Scheme 1: (i) excitation of the photosensitizer to its triplet state; (ii) energy transfer and (iii) dimerization. We studied the effect of methyl substitution on the $E(T_1)$ of conjugated dienes and on the activation and reaction energies of the step that leads to the dimer radical pair intermediate (first product of step iii in Scheme 1).

In their T_1 states, the acyclic conjugated dienes can be described as triplet radical pairs composed of two non-interacting radicals oriented perpendicularly to each other; one alkyl radical and one allyl radical (Figs. 4A and S6, ESI). The product of the first reaction step, on the other hand, can

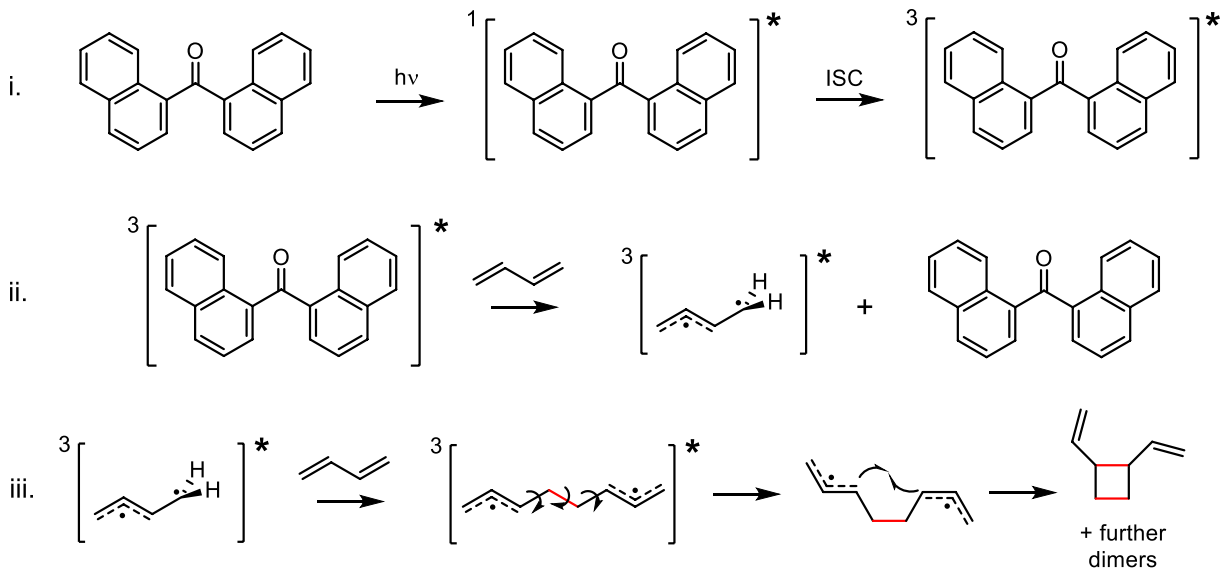

Scheme 1 Three main steps in the reaction mechanism of the photosensitized dimerization of conjugated dienes: (**i**) the excitation of the photosensitizer (1,1-dinaphthylmethanone) to its triplet state; (**ii**) the energy transfer from the photosensitizer to a ground state diene; (**iii**) the dimerization step, started by the attack of a T_1 diene to an S_0 diene, leading to a cyclic product after cyclization of the *bis*(allyl) radical pair intermediate, here exemplified on the simplest diene 1,3-butadiene. The product shown is only one of possible dimers (4-, 6-, and 8-membered rings, depending on the radical combinations in the final step). The bonds formed during the reaction are depicted in red. *ISC* intersystem crossing

be described as a *bis*(allyl) radical pair dimer with triplet multiplicity (Fig. 4B), a short-lived intermediate that undergoes intersystem crossing to the singlet radical pair and then closes to the observed dimers. Yet, when in their singlet state, the *bis*(allyl) radical pairs may also, in a competing reaction, dissociate via cleavage of the central C–C bond, which leads back to two diene reactants (see further below).

The methyl substituents have two effects: they hyperconjugatively stabilize the alkyl and allyl radicals that develop in the T_1 state diene; however, the more the methyl substituents, the more extensive is the steric congestion at the transition state that leads to the dimer radical pair intermediate. For the triplet state dienes and the dimer radical pair intermediates at their least congested (most stable) conformers, the methyl substituents only provide hyperconjugative stabilization. The steric effects, on the other hand, play a role at the transition states. The first three acyclic dienes (**1**–**3**) adopt lowest energy conformers described as one primary alkyl radical and one allyl radical, whereas **4**–**6** adopt triplet state conformers described as one secondary alkyl radical and one allyl radical.

So why does isoprene give the highest yield among the acyclic dienes? The yields decrease both when a second methyl group is attached to a central C atom of **2** leading to **3** and when the methyl group of **2** is removed leading to **1**. First, we consider the relative $E(T_1)$ of **1**–**3** (0.6, 0.0, and 0.3 kcal mol^{-1}, respectively), which do not reveal a gradual stabilization of the T_1 state with increasing methyl substitution. In the most stable conformer of ^{3}**2**, the methyl group is positioned at one of the ends of the allyl radical (at the inner end). In ^{3}**3**, both methyl groups are bonded to the internal C atoms, and one of these groups will be attached to the C2 atom of the allyl moiety of ^{3}**3**. At this position, the singly occupied molecular orbital (SOMO) has no coefficient, and this methyl group provides no additional stabilization when compared to **2**. One should also compare the two isomers **2** and **4**, and although $E(T_1)$ of **4** and **2** are the same, the methyl group in the most stable conformer of ^{3}**4** sits at the alkyl radical moiety in contrast to ^{3}**2** where it must sit at the allyl radical. Finally, when going to the dimethyl substituted **5** and **6**, one can note lowered $E(T_1)$ for some of the isomers. However, for *Z*,*Z*-**5** and *Z*-**6,** these should stem from destabilizing steric congestion in the S_0 state. Yet, the $E(T_1)$ is also low for *E*-**6** where the low energy instead reveals hyperconjugative stabilization of both the alkyl and the allyl radical moieties of the T_1 state.

Differences in the rate constants of triplet quenching have earlier been observed among different dienes as quenchers [48], and Sandros and Bäckström concluded that the triplet energy transfer is a diffusion-controlled process [49]. Changes in the steric hindrance of the photosensitizer have also been shown to not affect the energy transfer from carbonyl compounds to different substrates [50]. We previously identified the rate-determining step to be the addition of a T_1 state diene to an S_0 state diene leading to the triplet *bis*(allyl) radical pair intermediate [10]. The most reactive part of each

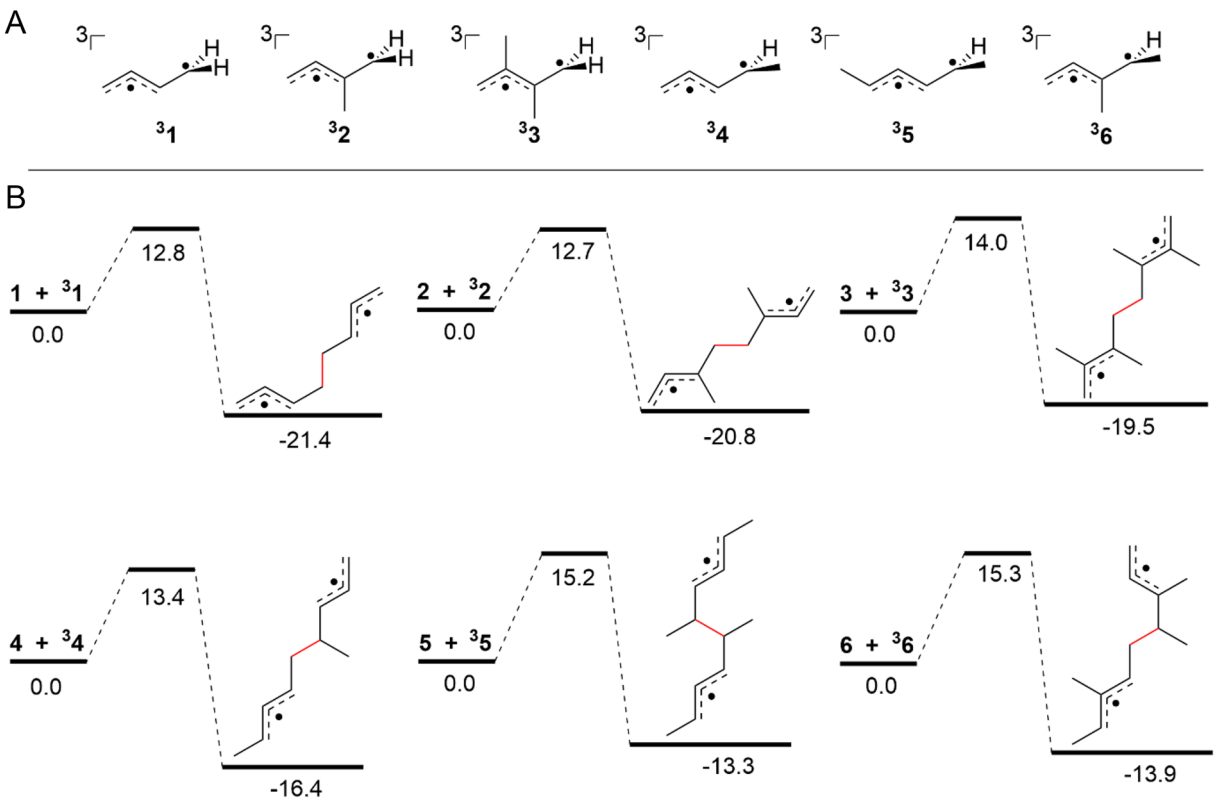

Fig. 4 **A** Schematic drawings of the most stable conformers of T_1 state dienes **1**–**6** based on the optimized (U)B3LYP-D3/6–311 + G(d,p) geometries. **B** Activation energies (kcal mol^{-1}) for the addition of a T_1 diene to an S_0 diene leading to a *bis*(allyl) radical pair intermediate, computed at (U)B3LYP-D3/6–311 + G(d,p) level as Gibbs free energies at 298 K. The chosen conformers of the T_1 diene and the S_0 diene are the most stable ones, combined to give the least steric congestion at the transition state and presumably the lowest activation barrier

triplet 1,3-diene is the alkyl radical moiety. Given the various possible conformers of the two reactants, we consider the reaction path when the T_1 state diene in its most stable conformer adds to an S_0 state diene in its most stable conformer, and we discuss the paths with the least steric congestion between the two reactants which should lead to the lowest activation barriers. In the case of **5** and **6**, the S_0 state conformers considered were the most stable ones of the *E*- and *E*,*E*-isomers. Furthermore, two orthogonally twisted T_1 state structures are possible for each of **2**, **4**, and **6** as these dienes can be twisted about either the C_1–C_2 or C_3–C_4 bond (Fig. 4).

First, the activation energies for the addition of ^{3}**1** and ^{3}**2** to the corresponding S_0 dienes are lower than those of **3**–**6**. For **4**–**6** the reactive alkyl radical site is a secondary radical, which explains the slightly higher activation barriers for these dienes. On the other hand, the higher activation energy and lower dimerization yield of **3**, as compared to **2**, could result from larger steric congestion at the transition state of the dimerization of **3**. This can be seen in several properties. First, the reactant molecule ^{3}**3** at the transition state for dimerization of **3** is more distorted than the reactant molecule ^{3}**2** at the transition state for dimerization of **2** (calculated distortion energies for ^{3}**3** and ^{3}**2** are, respectively, 3.1 and 1.7 kcal mol^{-1}). This is corroborated with the fact that the transition state of the photodimerization of **3** exhibits a shorter C–C bond-forming distance than what is the case for **2** (Fig. 5), simultaneously as the hydrogens from the two dienes are further apart in the case of **3** (Fig. S7, ESI). However, the reason for the lower reactivity of **1**, which we observed experimentally, is not clear as its computed activation energy resembles that of **2**. It may be a result of a slightly larger energy difference in the $E(T_1)$ of 1,1-dinaphthylmethanone sensitizer and **1** than between this sensitizer and **2**. In addition, the bond formed in the *bis*(allyl) radical pair of **1** is 0.009 Å longer than in the one of **2** (Fig. 5). Here, one may argue that the longer the bond distance, the more favorable it should be with a C–C bond cleavage, leading back to the starting diene reactants. Indeed, a more facile bond cleavage in **1** than in **2** may explain the lower dimer yield in the reaction of **1** compared to **2**. In fact, all the acyclic dienes except **6** show a correlation between the C–C bond distance and the yield of dimerization (Fig. S8, ESI), suggesting that this competing reaction occurs.

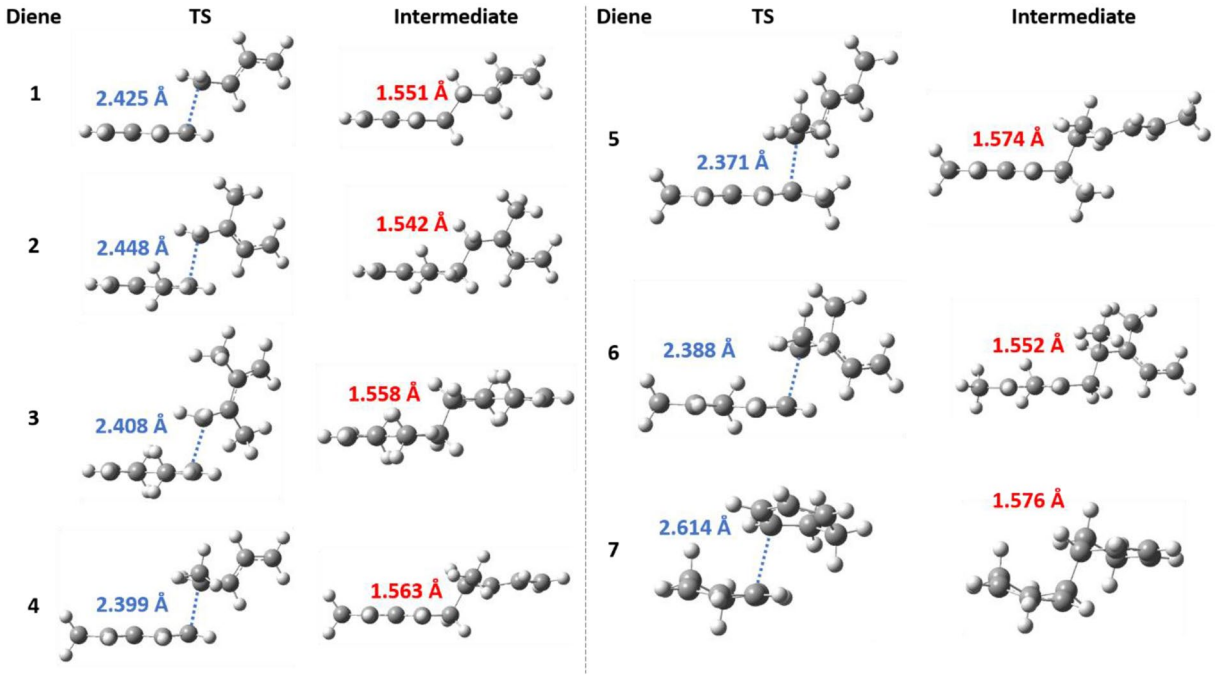

Fig. 5 Structures of transition states (TS) and *bis*(allyl) dimer radical pair intermediates formed in the addition of one T_1 diene to an S_0 diene calculated at (U)B3LYP-D3/6-311 + G(d,p) level. The bond distances of the forming bonds in the TS (blue) and intermediates (red) are indicated

Of the two isomers **2** and **4**, diene **4** has a 0.7 kcal mol^{-1} higher activation barrier than **2** for the first dimerization step, which should stem from the fact that the reactive alkyl radical part is a secondary radical in ^{3}**4**. This explains the lower dimerization yield of **4** than of **2**.

For the three dienes **4**–**6**, which have most stable conformers with secondary alkyl radical moieties, there are higher-energy conformers with primary alkyl radical moieties. For **4**, such a conformer is at a relative energy 0.7 kcal mol^{-1} above that most stable one, while for **6** such a conformer is less accessible at 2.8 kcal mol^{-1} above the most stable. In this less stable conformer of **6** with primary radical sites, the allyl radical moieties either experience steric congestion between methyl substituents on two adjacent C atoms or adopt a less favorable *Z*-configuration of the methyl substituted allyl radical. Thus, conformers with reactive primary alkyl radical moieties are less populated in the case of **6** (Fig. S9, ESI). In diene **5**, the methyl substituents are placed at the ends of the diene segment, and as a result, the alkyl radical moiety of this diene in its T_1 state will always be a secondary radical moiety.

The reaction energies become gradually less exergonic when going from **1** to **5** and **6**, which in part can be described by an increased hyperconjugative stabilization of the triplet diene reactants. In ^{3}**1**, there is no hyperconjugative stabilization, while in **5** and **6** the triplet dienes experience hyperconjugative methyl group stabilization of both the alkyl and allyl radical moieties. Accordingly, the gain in energy upon dimerization is smaller in the latter species. A second contributing factor may be a greater loss in entropy in the dimerization of **5** and **6** than of **1**, as the products of the two first dienes will be more structurally confined due to steric clashing between methyl substituents.

The activation energies of the rate-determining steps of **1**–**6** correlate moderately with the reaction energies ($R^2 = 0.80$, Fig. S10A, ESI), i.e., the more exergonic the addition step, the lower is the activation barrier, in line with the Bell–Evans–Polanyi principle [51, 52]. Furthermore, the computed spin densities in the transition state structures show a clear distinction between the reacting diene in its T_1 state and the reacting diene in its S_0 state (Fig. S11, ESI), as well as the spin polarization effect which the former has on the latter. These results reveal a reactant-like transition state, in line with the exergonic reaction profiles (Fig. 4).

Noteworthy, the even more substituted 2,5-dimethyl-2,4-hexadiene, where the T_1 state would be described as composed of a tertiary alkyl radical and a terminally dimethyl substituted allyl radical, has been reported to not form dimers when the sensitized photodimerization is attempted [11]. This supports our observation of a relationship between the reactivity of 1,3-dienes in these photoreactions and the extent of methyl substitution at or near the reactive C atom of the alkyl radical moiety. Isoprene (**2**) in T_1 is the most reactive diene because it is the mono-methyl substituted diene with a reactive alkyl radical moiety being a primary

alkyl radical. Its isomer, piperylene (**4**), is less reactive as its most stable conformer in the T_1 state has a secondary alkyl radical moiety. The dimethyl substituted dienes are all considerably less volatile and/or have less reactive secondary alkyl radical moieties.

3.2 Cyclic 1,3-dienes

The T_1 state of **7** has the dominant radical character at the two terminal C atoms of the conjugated diene segment (Fig. 6A, B), and this diene gives the highest yield of dimers after 24 h of irradiation (93%). After 12 h, the yield of dimers was already 80 wt.%, while it reached 95 wt.% after 36 h. Clearly, **7** has feature(s) not accessible to the acyclic 1,3-dienes which lead to faster kinetics.

Indeed, the much faster photodimerization of **7** than of **2**–**6** should (in part) result from its long T_1 state lifetime of 1.3–6.0 µs [53], which is two orders of magnitude longer than those of **2** and **5** being 27 and 32 ns, respectively. [53] Moreover, because of the planar T_1 state structure, ^{3}**7** is best described as two localized radicals at C1 and C4, localized to these atoms due to Pauli repulsion between the two same-spin electrons in the planar π-orbital system. Thus, there being two causes of the rapid photodimerization of **7**; (i) it has a long triplet lifetime, since it has fewer deactivation pathways due to the geometrically confined six-membered ring [54], and (ii) its two radicals are fairly localized in a 1,4-diradical leading to a higher reactivity. Cyclic conjugated dienes with larger and more flexible rings should have shorter T_1 lifetimes, and for **8** and **9** they are 400–550 and 40–120 ns, respectively [54, 55]. From the calculated T_1 state structures of the cyclic dienes **7**–**9** (Fig. 6C), the gradual change toward the structure of an acyclic diene becomes clear.

Triplet cyclohexadiene ^{3}**7** has C_2 symmetry so that the H–C1–C2–H and H–C3–C4–H dihedral angles are both 9.3°. In contrast, ^{3}**8** can exists in two different conformers: the most stable being a non-twisted C_s symmetric conformer with both terminal H–C–C–H dihedral angles of 6.5°, and a second conformer at a relative energy of 2.3 kcal/mol with an H–C–C–H dihedral angle of 77.4° and a planar allyl radical fragment. Finally, ^{3}**9** exists only as a twisted conformer described as one alkyl radical and one allyl radical moiety, and with one H–C–C–H dihedral angle of 80.8°. Similar results have been found by Allonas et al. [55], although the twisted conformer of ^{3}**8** (^{3}**8′**) was not noted in their work.

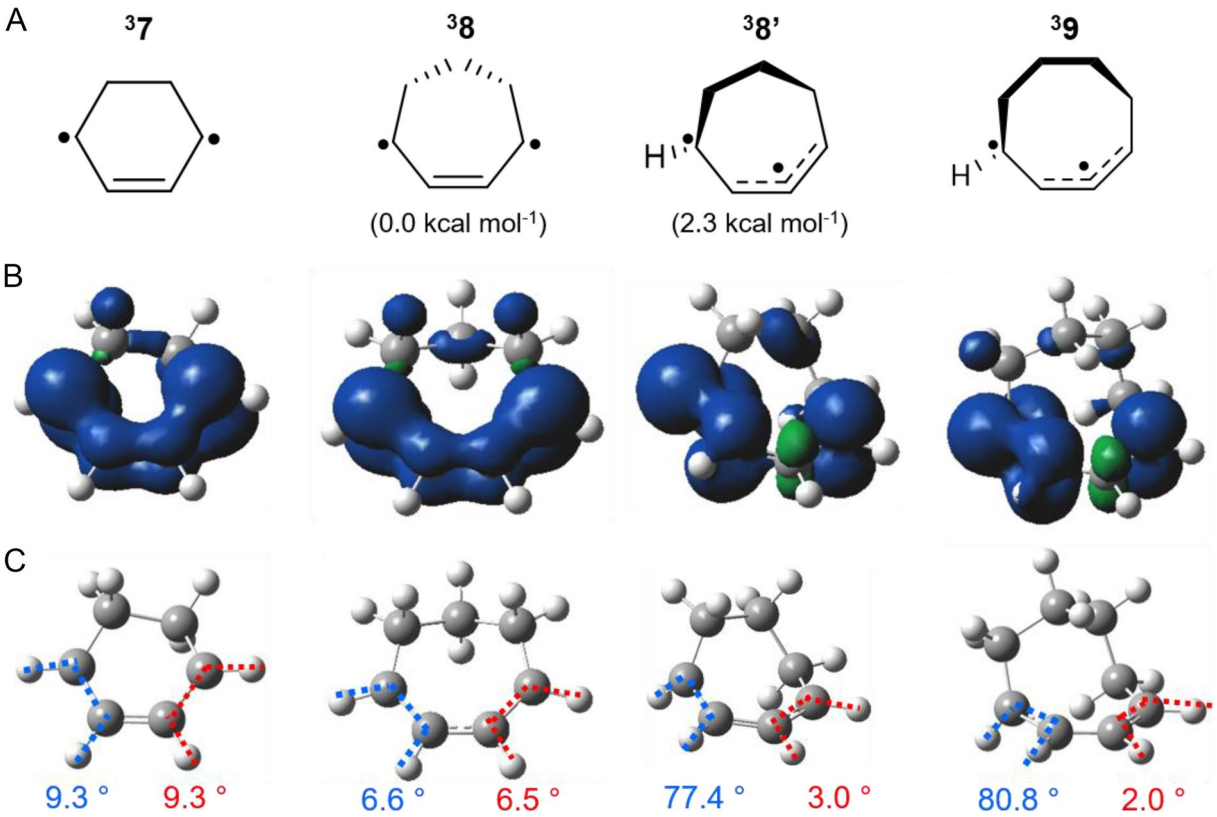

Fig. 6 **A** Geometries of the cyclic 1,3-dienes **7** – **9** in their T_1 states (two conformers of **8**; **8** and **8'**, respectively), calculated at the (U)B3LYP-D3/6–311 + G(d,p) level, **B** their spin densities (isovalue = 0.004), and **C** dihedral angles (written in red and blue). For 1,3-cycloheptadiene, two minima were found, and their relative free energies are shown in parentheses

Indeed, ^{3}**8'** may be the conformer from which decay to S_0 occurs. In ^{3}**9**, the level of twisting is comparable to what is found in the acyclic 1,3-dienes in their T_1 state (Fig. S12, ESI), and, consequently, its lifetime resembles those of acyclic triplet dienes. Both the shorter triplet lifetimes and the gradual decrease of spin density localized at the two terminal C atoms of the diene units (Fig. 6B) should reduce the efficiency of the sensitized photodimerization of cyclic 1,3-dienes as the ring size increases. Now, how is this reflected in the activation barriers?

As seen in Fig. 7, the activation barriers become higher and the dimerization steps become less exergonic as the ring size increases. Yet, the activation energy for the first dimerization step of **7** is even lower than those of **1** and **2**, a result of higher reactivity of the non-twisted ^{3}**7**, a planar 1,4-diradical, with Pauli repulsion between the two same-spin electrons. On the other hand, the reaction of **7** is less exergonic than those of **1** and **2**, which relates to the more congested diradical intermediate formed in the case of **7**. In addition, the longer T_1 lifetime contributes for the more rapid dimerization of **7,** as it leads to a higher concentration of ^{3}**7** than of other 1,3-dienes in their T_1 states. By assuming

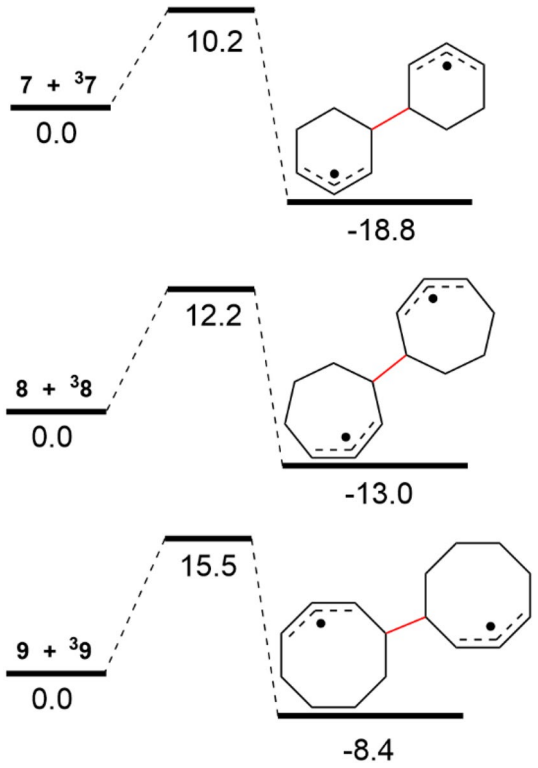

Fig. 7 Activation barriers of the addition of a T_1 state diene to an S_0 state diene to form *bis*(allyl) radical pair intermediates, for dienes **7**–**9**. Calculated at (U)B3LYP-D3/6-311 + G(d,p) level as Gibbs free energies at 298 K. The energy barriers and relative energy of the intermediates formed are in kcal mol^{-1} and they are relative to the energy of the reactants

that every encounter between the T_1 photosensitizer and **7** is successful for the energy transfer, and that these encounters are diffusion controlled (see the ESI), we estimate the concentrations of T_1 state species as: $[^{3}\mathbf{7}] = 8.3 \times 10^{-7}$ M, $[^{3}\mathbf{8}] = 2.6 \times 10^{-7}$ M, $[^{3}\mathbf{9}] = 2.6 \times 10^{-8}$ and $[^{3}\mathbf{2}] = 1.7 \times 10^{-8}$ M (see the ESI, Sect. 1.2). Thus, the concentration of ^{3}**7** is 3 to nearly 50 times higher than the ones calculated for the two larger cyclic dienes and for isoprene.

Hence, we tested the sensitized photodimerization of the larger **8** and **9** under the same conditions as **7**, leading to yields of, respectively, 45% and 7% (Table 1). Clearly, as the degree of twisting in the T_1 state increases, the yield of dimers decreases, confirming that the twisting of the larger cyclic 1,3-dienes in their T_1 states reduces the efficiency of the photosensitized dimerization. In fact, for **9** the yield is comparable to that of **5**. Interestingly, **8** shows a lower yield of dimers than **2** despite having a significantly longer triplet lifetime (~ 500 vs. 27 ns). With regard to the reactions of **8** and **9**, it should be noted that trace amounts of intramolecular cyclization products were observed (Fig. S13, ESI).

Taken together, the results indicate that 1,3-cyclohexadiene and isoprene are the most suitable substrates in the photodimerizations. If one plots the activation energies of the first dimerization steps of **1**–**9** against the corresponding reaction energies, one sees that **7** and **8** are outliers (Fig. S10B, ESI). With **7** and **8** included, an R^2 value of 0.32 is obtained for a linear regression, whereas a value 0.79 is found without these compounds. Dienes **7** and **8** have a lower activation energy than predicted from the fit, a fact that should stem from their localized 1,4-diradical characters.

We now proceed to further explore the optimal reaction conditions.

3.3 Effects of diene and sensitizer concentrations on photodimerization yields

Earlier herein, we irradiated hexane solutions of isoprene (15 wt%) to enable a comparison with the corresponding results for 1,3-butadiene. We now tested different concentrations of isoprene solutions (5–60 wt% in hexane) keeping a constant photosensitizer concentration (0.1 mol%) to explore how dilution affects the dimerization yield. Low isoprene concentrations are interesting as they resemble the dilute solutions that result when photobiologically produced isoprene is trapped. As seen in Fig. 8A, the yield of dimers decreases linearly with decreased isoprene concentrations.

We also explored the impact of increasing the photosensitizer concentrations (0.1–0.6 mol%) using a hexane solution of isoprene (15% in hexane). An increased sensitizer concentration should favor the bimolecular triplet energy transfer, and as seen in Fig. 8B, the yield of isoprene

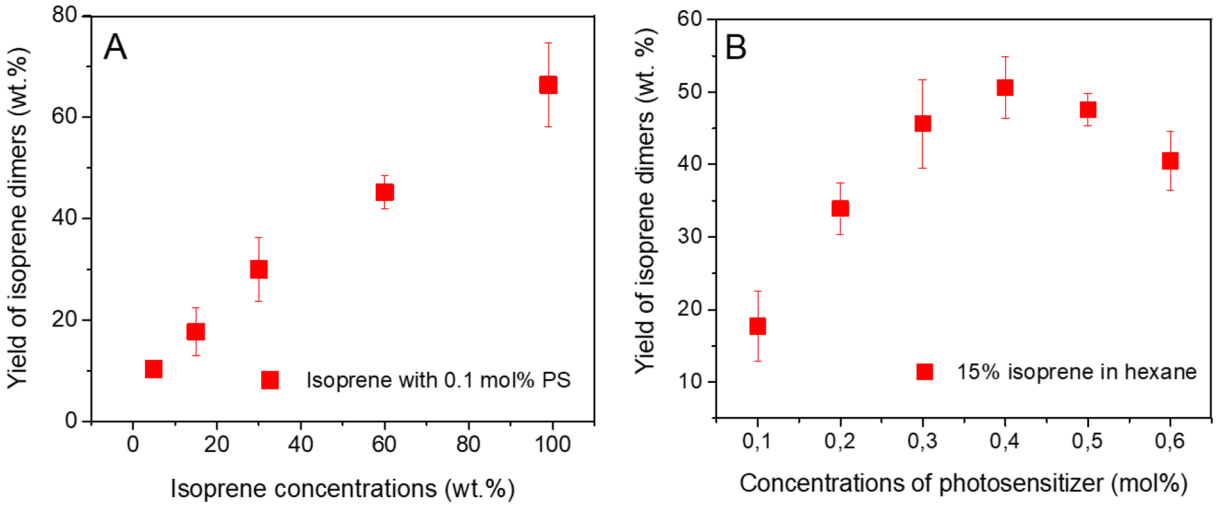

Fig. 8 Effects of concentrations of isoprene and 1,1-dinaphthylmethanone on the photodimerization yields. **A** The total yield of dimers (wt%) as a function of isoprene concentration (5–99 wt% in hexane) with 1,1-dinaphthylmethanone (0.1 mol%, related to the isoprene concentration). **B** The total yield of dimers from the photodimerization of 15% isoprene in hexane as a function of 1,1-dinaphthylmethanone concentration (0.1–0.6 mol%)

dimers increased by up to a value of 54% with 0.4 mol% of 1,1-dinaphthylmethanone. This is almost three times higher than in the reaction using the solution with 0.1 mol% photosensitizer. However, with 0.5 and 0.6 mol% photosensitizer the dimer yields dropped, a result of either self-quenching between two photosensitizer molecules or quenching of ^{3}**2** by a photosensitizer molecule. Although endergonic, the latter may occur given that the $E(T_1)$ of isoprene is close to that of the sensitizer [49]. Thus, a loading of 0.4 mol% is the optimal photosensitizer loading in the diluted condition of 15 wt.% isoprene in hexane. We also tested the neat isoprene (99%) with a higher concentration of photosensitizer (0.4 mol%), but in this case, the yield of dimers did not increase when compared to the 0.1 mol% case (Table S1, ESI). Thus, increasing the photosensitizer concentration will improve the efficiency of the photodimerization in dilute isoprene concentrations, but not in more concentrated ones.

3.4 Solvent viscosity and dimerization yield

The photosensitized dimerization of 1,3-cyclohexadiene in solution has been shown to be viscosity dependent, with an increase in the yield of dimers as the pressure and, consequently, the viscosity of the solvent increases [56]. The decay from the T_1 state also has a dependence on the solvent viscosity at low viscosity ranges [57], behaving as a diffusion-limited process. For this reason, we tested solvents with different viscosities (hexane (0.3 cP), cyclohexane (1.0 cP), tetradecane (2.3 cP), and hexadecane (3.4 cP)), and carried out irradiation experiments (24 h) on solutions of isoprene in these solvents (15 wt%) and with 0.1 mol% of 1,1-dinaphthylmethanone. The relative yields of dimers were assessed by ^{1}H NMR spectroscopy (Table 2, Fig. S14, ESI), based on the ratio of the integration of protons from the starting material isoprene and the protons of the dimers formed.

Table 2 Effect of different viscosity of solvents on photodimerization of isoprene (15 wt%, and 0.1 mol% 1,1-dinaphthylmethanone). Samples were irradiated for 24 h

Solvents	Viscosity (cP at 20–25 °C)	Relative integration of dimers signal (%)
Hexane	0.3	60
Cyclohexane	1.0	48
Tetradecane	2.3	41
Hexadecane	3.4	43

In contrast to earlier observations by Liu et al. [15], our results show that the yield of isoprene dimers is indeed affected by a change in solvent viscosity; however, there is not a linear dependence on the viscosity over the range we chose. In fact, the yield decreases when going from hexane (0.3 cP) to cyclohexane (1.0 cP) and tetradecane (2.3 cP), but slightly increases again when going to hexadecane (3.4 cP). Just like the T_1 decay dependence upon solvent viscosity, the yield of isoprene dimers is viscosity-dependent only for a low range of viscosity values. Among the ones studied herein, hexane is clearly the optimal solvent with a somewhat higher dimerization efficiency than the other alkane solvents.

4 Conclusions

Through comparisons of the photosensitized dimerization of various conjugated dienes, we could identify how different electronic and structural factors affect their reactivities. Being the most reactive, the photodimerization of 1,3-cyclohexadiene is favored both by its long T_1 lifetime and its more reactive triplet with a 1,4-diradical character. Thus, pathways to photobiological production of 1,3-cyclohexadiene should be sought, although a drawback is its nonvolatility (b.p. = 80 °C) making it unusable in our previously reported two-step photobiological–photochemical approach to jet fuel hydrocarbons.

Among the acyclic conjugated dienes, isoprene gave the highest yield of dimers. Importantly, and in contrast to 1,3-cyclohexadiene, isoprene is volatile enough to escape from the cyanobacteria cells, facilitating its harvest. Yet, it is still a liquid at room temperature, which makes it facile to handle in the photochemical dimerization step. Such advantages put isoprene as the ideal 1,3-diene in our two-step photobiological–photochemical route to jet fuels. The smallest conjugated diene, 1,3-butadiene, has a lower photoreactivity and is a gas at ambient temperature (b.p. −4 °C). The lower reactivities of other linear conjugated dienes result from their higher number of methyl substituents and their radical character in the T_1 state structures being placed in internal carbons, which leads to more hindered radicals and provide for hyperconjugative stabilization. Indeed, our results showed that the methyl substitution patterns affect the photosensitized dimerization of 1,3-dienes, while the large difference in the triplet lifetimes dominates the effects for cyclic 1,3-dienes.

The trapping of photobiologically produced dienes will likely be in alkane solvents. As the dilution of dienes reduces the yields of dimerization, we explored raising the photosensitizer loading, which improved the conversions, until an optimal loading is reached after which the conversion decreased. The results support further development of our two-step photobiological–photochemical production of jet fuel hydrocarbons via small 1,3-dienes, with a special focus on isoprene as the most suitable diene as it is readily available photobiologically and known to undergo a highly efficient photosensitized dimerization.

Supplementary Information The online version contains supplementary material available at https://doi.org/10.1007/s43630-023-00418-0.

Acknowledgements We greatly acknowledge the Swedish Energy Agency for financial support of the present project through Grant 52576-1. Assoc Profs. Pia Lindberg, Karin Stensjö, and Prof. Peter Lindblad are acknowledged for encouraging the multidisciplinary collaboration between bioengineering and organic photochemistry for the development of biojet fuel at Uppsala University. The computations were enabled by resources provided by the Swedish National Infrastructure for Computing (SNIC) at the National Supercomputer Center (NSC), Linköping, partially funded by the Swedish Research Council through Grant agreement number 2018-05973.

Funding Open access funding provided by Uppsala University.

Data availability All original data generated in this study is included in the main article and the Supplementary Information.

Declarations

Conflict of interest There are no conflicts of interests.

References

1. Chevron Products Company, *Aviation Fuels—Technical Review*, 2007.
2. Wilson, J., Gering, S., Pinard, J., Lucas, R., & Briggs, B. R. (2018). *Biotechnology for Biofuels, 11*, 1–11.
3. Angelici, C., Weckhuysen, B. M., & Bruijnincx, P. C. A. (2013). *ChemSusChem, 6*, 1595–1614.
4. Kang, M. K., & Nielsen, J. (2017). *Journal of Industrial Microbiology and Biotechnology, 44*, 613–622.
5. Rodrigues, J. S., Lindberg, P. (2021). Engineering cyanobacteria as host organisms for production of terpenes and terpenoids. Cyanobacteria Biotechnology 267–300.
6. Rodrigues, J. S., & Lindberg, P. (2021). Metabolic engineering of Synechocystis sp. PCC 6803 for improved bisabolene production. *Metabolic Engineering Communications, 12*, e00159.
7. Betterle, N., & Melis, A. (2019). Photosynthetic generation of heterologous terpenoids in cyanobacteria. *Biotechnology and Bioengineering, 116*, 2041–2051.
8. Formighieri, C., & Melis, A. (2018). Cyanobacterial production of plant essential oils. *Planta, 248*, 933–946.
9. Keasling, J., Garcia Martin, H., Lee, T. S., Mukhopadhyay, A., Singer, S. W., & Sundstrom, E. (2021). Microbial production of advanced biofuels. *Nature Reviews Microbiology, 19*, 701–715.
10. Rana, A., Cid Gomes, L., Rodrigues, J. S., Yacout, D. M. M., Arrou-Vignod, H., Sjölander, J., Vedin, N. P., El Bakouri, O., Stensjö, K., Lindblad, P., Andersson, L., Sundberg, C., Berglund, M., Lindberg, P., & Ottosson, H. (2022). A combined photobiological-photochemical route to C_{10} cycloalkane jet fuels from carbon dioxide via isoprene. *Green Chemistry, 24*, 9602–9619.
11. Liu, R. S.-H. (1965). California Institute of Technology.
12. Hammond, G. S., Turro, N. J., & Liu, R. S. H. (1963). Mechanisms of photochemical reactions in solution. XVI. 1 Photosensitized dimerization of conjugated dienes. *The Journal of Organic Chemistry, 28*, 3297–3303.
13. Valentine, D., Turro, N. J., & Hammond, G. S. (1964). Thermal and photosensitized dimerizations of cyclohexadiene. *Journal of the American Chemical Society, 86*, 5202–2508.

14. Mella, M., Fasani, E., & Albini, A. (1991). The photosensitized dimerization of 1,3-cyclohexadiene. *Tetrahedron, 47*, 3137–3154.
15. Liu, R. S. H., Turro, N. J., & Hammond, G. S. (1965). Mechanisms of photochemical reactions in solution. XXXI. Activation and deactivation of conjugated dienes by energy transfer. *Journal of the American Chemical Society, 87*, 3406–3412.
16. Muldoon, J. A., & Harvey, B. G. (2020). Bio–based cycloalkanes: the missing link to high–performance sustainable jet fuels. *ChemSusChem*, 13, 5777–5807.
17. Lindblad, P., Lindberg, P., Oliveira, P., Stensjö, K., & Heidorn, T. (2012). Design, engineering, and construction of photosynthetic microbial cell factories for renewable solar fuel production. *Ambio, 41*, 163–168.
18. Lau, N.-S., Matsui, M., Abdullah, A. A.-A. (2015). Cyanobacteria: Photoautotrophic microbial factories for the sustainable synthesis of industrial products. BioMed Research International. https://doi.org/10.1155/2015/754934
19. Thiel, K., Mulaku, E., Dandapani, H., Nagy, C., Aro, E. M., & Kallio, P. (2018). Translation efficiency of heterologous proteins is significantly affected by the genetic context of RBS sequences in engineered cyanobacterium Synechocystis sp. PCC 6803. *Microbial Cell Factories, 17*, 1–12.
20. Mustila, H., Kugler, A., & Stensjö, K. (2021). Isobutene production in Synechocystis sp. PCC 6803 by introducing α-ketoisocaproate dioxygenase from Rattus norvegicus. *Metabolic Engineering Communications, 12*, e00163.
21. Englund, E., Shabestary, K., Hudson, E. P., & Lindberg, P. (2018). Systematic overexpression study to find target enzymes enhancing production of terpenes in Synechocystis PCC 6803, using isoprene as a model compound. *Metabolic Engineering, 49*, 164–177.
22. Vajravel, S., Sirin, S., Kosourov, S., & Allahverdiyeva, Y. (2020). Towards sustainable ethylene production with cyanobacterial artificial biofilms. *Green Chemistry, 22*, 6404–6414.
23. Lyons, T. W., Guironnet, D., Findlater, M., & Brookhart, M. (2012). Synthesis of p-xylene from ethylene. *Journal of the American Chemical Society, 134*, 15708–15711.
24. Mori, Y., Noda, S., Shirai, T., & Kondo, A. (2021). Direct 1,3-butadiene biosynthesis in *Escherichia coli* via a tailored ferulic acid decarboxylase mutant. *Nature Communications, 12*, p2195.
25. Messiha, H. L., Payne, K. A. P., Scrutton, N. S., & Leys, D. (2021). A biological route to conjugated alkenes: Microbial production of hepta-1,3,5-triene. *ACS Synthetic Biology, 10*, 228–235.
26. Quinzler, D., & Mecking, S. (2010). Linear semicrystalline polyesters from fatty acids by complete feedstock molecule utilization. *Angewandte Chemie - International Edition, 49*, 4306–4308.
27. Mmongoyo, J. A., Mgani, Q. A., Mdachi, S. J. M., Pogorzelec, P. J., & Cole-Hamilton, D. J. (2012). Synthesis of a kairomone and other chemicals from cardanol, a renewable resource. *European Journal of Lipid Science and Technology, 114*, 1183–1192.
28. Mutlu, H., Hofsäß, R., Montenegro, R. E., & Meier, M. A. R. (2013). Self-metathesis of fatty acid methyl esters: Full conversion by choosing the appropriate plant oil. *RSC Advances, 3*, 4927–4934.
29. van Velzent, P. N. T., & van der Harts, W. (1984). The isomerization of 1,4mCyclohexadiene Ions to the 1,3=cyclohexadiene structure as studied by photodissociation. *Organic Mass Spectrometry, 19*, 190–192.
30. Mathers, R. T., Shreve, M. J., Meyler, E., Damodaran, K., Iwig, D. F., & Kelley, D. J. (2011). Synthesis and polymerization of renewable 1, 3-cyclohexadiene using metathesis, isomerization, and cascade reactions with late-metal catalysts. *Macromolecular Rapid Communications, 32*, 1338–1342.
31. Pingen, D., Zimmerer, J., Klinkenberg, N., & Mecking, S. (2018). Microalgae lipids as a feedstock for the production of benzene. *Green Chemistry, 20*, 1874–1878.
32. Sun, D., Li, Y., Yang, C., Su, Y., Yamada, Y., & Sato, S. (2020). Production of 1,3-butadiene from biomass-derived C_4 alcohols. *Fuel Processing Technology, 197*, 106193.
33. Hu, Y., Li, N., Li, G., Wang, A., Cong, Y., Wang, X., & Zhang, T. (2017). Solid acid-catalyzed dehydration of pinacol derivatives in ionic liquid: Simple and efficient access to branched 1,3-dienes. *ACS Catalysis, 7*, 2576–2582.
34. Sun, R., Zheng, M., Li, X., Pang, J., Wang, A., Wang, X., & Zhang, T. (2017). Production of renewable 1,3-pentadiene from xylitol via formic acid-mediated deoxydehydration and palladium-catalyzed deoxygenation reactions. *Green Chemistry, 19*, 638–642.
35. Liu, S., Qi, Y., Feng, R., Cui, L., Dai, Q., & Bai, C. (2021). Multifunctional Ce/ZrSi catalyst synergistically converting 1,4-pentanediol derived from levulinic acids to renewable pentadiene. *ACS Sustain Chem Eng, 9*, 8341–8346.
36. Yao, B., Xiao, T., Makgae, O. A., Jie, X., Gonzalez-Cortes, S., Guan, S., Kirkland, A. I., Dilworth, J. R., Al-Megren, H. A., Alshihri, S. M., Dobson, P. J., Owen, G. P., Thomas, J. M., & Edwards, P. P. (2020). Transforming carbon dioxide into jet fuel using an organic combustion-synthesized Fe-Mn-K catalyst. *Nature Communications, 11*, 6395.
37. Nicholas, C. P. (2017). Applications of light olefin oligomerization to the production of fuels and chemicals. *Applied Catalysis, A: General, 543*, 82–97.
38. Woodroffe, J.-D., & Harvey, B. G. (2022). Thermal cyclodimerization of isoprene for the production of high-performance sustainable aviation fuel. *Energy Advances, 1*, 338–343.
39. Rosenkoetter, K. E., Kennedy, C. R., Chirik, P. J., & Harvey, B. G. (2019). [4 + 4]-cycloaddition of isoprene for the production of high-performance bio-based jet fuel. *Green Chemistry, 21*, 5616–5623.
40. Cid Gomes, L., Rana, A., Berglund, M., Wiklund, P., & Ottosson, H. (2023). Light-driven (cross-)dimerization of terpenes as a route to renewable C_{15}–C_{30} crudes for fuel and lubricant oil applications. *Sustainable Energy & Fuels, 7*, 868–882.
41. Rajagopal, S. K., Nagaraj, K., Deb, S., Bhat, V., Sasikumar, D., Sebastian, E., & Hariharan, M. (2018). Extending the scope of the carbonyl facilitated triplet excited state towards visible light excitation. *Physical Chemistry Chemical Physics, 20*, 19120–19128.
42. Becke, A. D. (1993). Density-functional thermochemistry. III. The role of exact exchange. *The Journal of Chemical Physics, 98*, 5648–5652.
43. Lee, C., Yang, W., & Parr, R. G. (1988). Development of the Colle-Salvetti correlation-energy formula into a functional of the electron density. *Physical Review B, 37*, 785.
44. Stephens, P. J., Devlin, F. J., Chabalowski, C. F., & Frisch, M. J. (1994). Ab initio calculation of vibrational absorption and circular dichroism spectra using density functional force fields. *Journal of Physical Chemistry, 98*, 11623–11627.
45. Krishnan, R., Binkley, J. S., Seeger, R., & Pople, J. A. (1980). Self-consistent molecular orbital methods. XX. A basis set for correlated wave functions. *The Journal of Chemical Physics, 72*, 650–654.
46. Jovanovic, S. V., Morris, D. G., Pliva, C. N., & Scaiano, J. C. (1997). Laser flash photolysis of dinaphthyl ketones. *Journal of Photochemistry and Photobiology A: Chemistry, 107*, 153–8.
47. Saltiel, J., Metts, L., & Wrighton, M. (1969). Benzophenone-sensitized photoisomerization of the 2, 4-hexadienes in solution. *Journal of the American Chemical Society, 91*, 5684–5685.
48. Fry, A. J., Liu, R. S. H., & Hammond, G. S. (1966). Mechanisms of photochemical reactions in solution. XLI. Comparison of

rates of fast triplet quenching reactions. *Journal of the American Chemical Society, 88*, 4781–4782.
49. Sandros, K., & Bäckström, H. L. J. (1962). Transfer of Triplet State Energy in Fluid Solutions. *Acta Chemica Scandinavica, 16*, 958–968.
50. Wagner, P. J., McGrath, J. M., & Zepp, R. G. (1972). Sterically indifferent triplet energy transfer. *Journal of the American Chemical Society, 94*, 6883–6886.
51. Bell, R. P. (1936). The theory of reactions involving proton transfers. *Proceedings of the Royal Society of London. Series A-Mathematical and Physical Sciences, 154*, 414–429.
52. Evans, M. G., & Polanyi, M. (1938). Inertia and driving force of chemical reactions. *Transactions of the Faraday Society, 34*, 11–24.
53. Caldwell, R. A., & Singh, M. (1982). Lifetimes of conjugated diene triplets. *Journal of the American Chemical Society, 104*, 6121–6122.
54. Nakabayashi, K., Toki, S., & Takamuku, S. (1986). Triplet states of cyclic olefins and dienes. On the lifetimes and chemical reactivities studied by pulse radiolysis. *Chemical Letter, 15*, 1889–1892.
55. Allonas, X., Lalevée, J., & Fouassier, J. P. (2003). Influence of the S_0–T_1 structural changes on the triplet-triplet sensitization of dienes. *Chemical Physics, 290*, 257–266.
56. Chung, W.-S., Turro, N. J., Mertes, J., & Mattay, J. (1989). Pressure-induced diastereoselectivity in photoinduced diels-alder reactions. *Journal of Organic Chemistry, 54*, 4881–4887.
57. Lower, S. K., & El-Sayed, M. A. (1966). The triplet state and molecular electronic processes in organic molecules. *Chemical Reviews, 66*, 199–241.